

# A “Chimie Douce” Synthesis of Perovskite-Type $\text{SrTa}_2\text{O}_6$ and $\text{SrTa}_{2-x}\text{Nb}_x\text{O}_6$ <sup>1</sup>

Patricia J. Ollivier and Thomas E. Mallouk\*

Department of Chemistry,  
The Pennsylvania State University,  
University Park, Pennsylvania 16802

Received March 31, 1998  
Revised Manuscript Received June 29, 1998

“Chimie douce”, or soft chemistry, represents a simple and useful route to metastable solid-state compounds. These terms have historically been used to describe several types of low-temperature solid–solid transformations such as intercalation/deintercalation, ion exchange, hydrolysis, and redox reactions.<sup>2</sup> The common feature of soft chemical reactions is that they produce metastable compounds that are structurally related to the parent solid, by preserving the atomic connectivity of small building blocks and/or extended structural elements. Some interesting examples of unusual phases made by soft chemistry include  $\text{ReO}_3$ -like  $\text{MoO}_3$ ,<sup>3</sup>  $\text{Ti}_2\text{Nb}_2\text{O}_9$ ,<sup>4</sup> hexagonal  $\text{WO}_3$ ,<sup>5</sup>  $\text{TiO}_2\text{--B}$ ,<sup>6</sup>  $\text{VS}_2$ ,<sup>7</sup> and layered double hydroxides.<sup>8</sup> In general, it is not possible to prepare these compounds using high-temperature routes. Some of these low-temperature compounds have special properties, such as reversible intercalation, photoconductivity, or catalytic activity, which are not found in high-temperature, stable phases of the same composition.

We report in this paper a chimie douce reaction that converts a layered perovskite phase into a metastable three-dimensional perovskite. The topochemical transformation is illustrated in Figure 1. In this series of reactions, the lamellar compound  $\text{K}_2\text{SrTa}_2\text{O}_7$  and isostructural  $\text{K}_2\text{SrTa}_{2-x}\text{Nb}_x\text{O}_7$  ( $x = 0.2, 0.4$ ) are first ion-exchanged to the corresponding acid forms and then topochemically dehydrated to yield metastable perovskite phases  $\text{SrTa}_2\text{O}_6$  and  $\text{SrTa}_{2-x}\text{Nb}_x\text{O}_6$ . The process is similar to that previously reported for ion-exchange and condensation of  $\text{K}_2\text{Ln}_2\text{Ti}_3\text{O}_{10}$ .<sup>10</sup> Further heating causes the transformation to the structurally unrelated tetragonal tungsten bronze phases of the same composition. This transformation is interesting because  $\text{K}_2\text{--SrTa}_2\text{O}_7$  is a member of a large class of structurally related compounds<sup>9</sup> (the Ruddlesden–Popper phases,

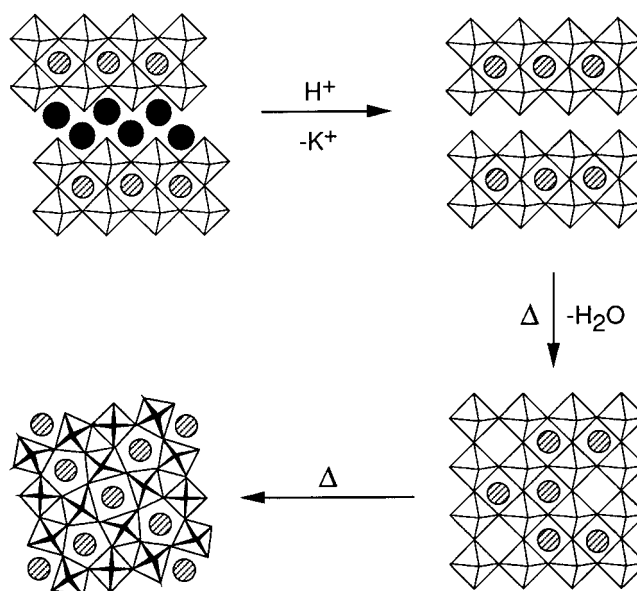


**Figure 1.** Schematic structural drawing of the transformations from Ruddlesden–Popper to perovskite to TTB phases.

$\text{A}_2\text{M}_n\text{M}'_{n+1}\text{O}_{3n+4}$ ,  $n = 1\text{--}4$ ), which could in principle undergo similar reactions to form metastable perovskites  $\text{M}_n\text{M}'_{n+1}\text{O}_{3n+3}$ . Since some perovskites have useful physical properties, such as superconductivity, colossal magnetoresistance, and ferroelectricity, this reaction may provide a route to interesting materials that are inaccessible through high-temperature synthesis.

Ion exchange of  $\text{K}_2\text{SrTa}_{2-x}\text{Nb}_x\text{O}_7$  ( $x = 0.0, 0.2, 0.4$ )<sup>11</sup> was carried out in water by slowly titrating the stirred suspension with 0.5 M HCl to a pH of 6–7. If the pH is allowed to drop below 6, hydrolysis occurs, as evidenced by apparent loss of crystallinity in the X-ray powder pattern. Complete exchange typically required 2–3 days of stirring. The X-ray powder diffraction pattern of  $\text{H}_2\text{SrTa}_{2-x}\text{Nb}_x\text{O}_7$  ( $x = 0.4$ ) was indexed to a tetragonal phase,  $a = 3.89(4)$ ,  $c = 9.87(18)$  Å. (Figure 2 and Table 1). The  $c$  axis dimension is halved upon proton exchange, because of a lateral shift of alternate layers, as shown in Figure 1. This effect has been previously observed in the proton exchange of other hydrated Ruddlesden–Popper and Dion–Jacobson phases.<sup>8a</sup>

Upon heating,  $\text{H}_2\text{SrTa}_{2-x}\text{Nb}_x\text{O}_7$  gradually loses water, and the progression of layer lines ( $00l$ ) in the powder pattern is lost, leaving the observed perovskite pattern. The metastable phase  $\text{SrTa}_{2-x}\text{Nb}_x\text{O}_6$  appears at 350–

(1) In fond memory of Professor Jean Rouxel.

(2) (a) Rouxel, J.; Tournoux, M. *Solid State Ionics* **1996**, *84*, 141. (b) Gopalakrishnan, J. *Chem. Mater.* **1995**, *7*, 1265. (c) Schleich, D. M. *Solid State Ionics* **1994**, *70/71*, 407.

(3) (a) Figlarz, M. *Prog. Solid State Chem.* **1989**, *19*, 1. (b) McCarron, E. M. *J. Chem. Soc., Chem. Commun.* **1986**, 336.

(4) Rebbah, H.; Desgardin, G.; Raveau B. *Mater. Res. Bull.* **1979**, *24*, 1125.

(5) (a) Gérard, B.; Seguin, L. *Solid State Ionics* **1996**, *84*, 199.

(6) (a) Marchand, R.; Brohan, L.; Tournoux, M. *Mater. Res. Bull.* **1980**, *15*, 1129. (b) Feist, T. P.; MocarSKI, S. J.; Davies, P. K.; Jacobson, A. J.; Lewandowski, J. T. *Solid State Ionics* **1988**, *28–30*, 1338. (c) Feist, T. P.; Davies, P. K. *J. Solid State Chem.* **1992**, *101*, 275.

(7) Murphy, D. W.; Cros, C.; DiSalvo, F. J.; Waszczak, J. V. *Inorg. Chem.* **1977**, *16*, 3027.

(8) Delmas, C.; Borthomieu, Y. *J. Solid State Chem.* **1993**, *104*, 345.

(9) (a) Ruddlesden, S. N.; Popper, P. *Acta Crystallogr.* **1957**, *10*, 538; *Acta Cryst.* **1958**, *11*, 54. (b) Uma, S.; Raju, A. R.; Gopalakrishnan, J. *J. Mater. Chem.* **1993**, *3*, 709.

(10) Gopalakrishnan, J.; Bhat, V. *Inorg. Chem.* **1987**, *26*, 4301.

(11)  $\text{K}_2\text{SrTa}_{2-x}\text{Nb}_x\text{O}_7$  was prepared by the solid-state reaction of the constituent oxides and carbonates. Stoichiometric quantities of  $\text{SrCO}_3$ ,  $\text{Ta}_2\text{O}_5$ , and  $\text{Nb}_2\text{O}_5$  were ground with a 150% molar excess of  $\text{K}_2\text{CO}_3$  and pressed into pellets at 1000 psi pressure. The pellets were heated to 850 °C for 1 h and 1050 °C for 12 h. After the first heating cycle, the reaction was not complete, so the reactants were again heated for 1 h at 850 °C and 12 h at 1150 °C. After the second heating cycle, the two-layer Ruddlesden–Popper phase  $\text{K}_2\text{SrTa}_{2-x}\text{Nb}_x\text{O}_7$  was obtained, and the X-ray powder diffraction pattern was compared to a simulated pattern (Eutax). All peaks were indexed to the simulated pattern. The phase purity was estimated to be 85–90%, the remainder being a perovskite phase.

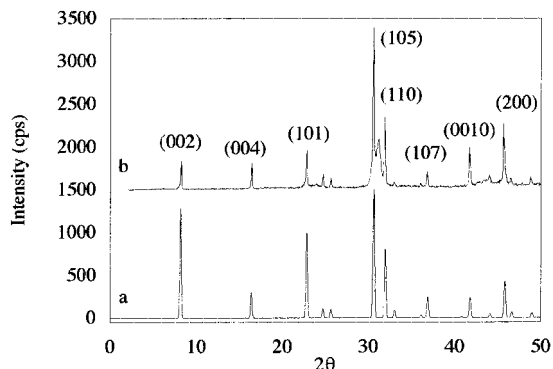


**Figure 2.** X-ray powder diffraction patterns showing Ruddlesden–Popper to perovskite to TTB phase transformations: (a) simulated and (b) observed patterns for  $K_2SrTa_{1.6}Nb_{0.4}O_7$ .

**Table 1. Indexing of X-ray Powder Diffraction Data**

| <i>h k l</i>   | <i>d</i> (obs) | <i>d</i> (calc) | <i>I</i> <sub>rel</sub> |
|--|----------------|-----------------|-------------------------|
| <b><math>K_2SrTa_{1.6}Nb_{0.4}O_7</math> Ruddlesden–Popper Phase</b>       |                |                 |                         |
| <i>(a</i> = 3.96(3), <i>c</i> = 21.5(3))                                   |                |                 |                         |
| 0 0 2  | 10.714         | 10.81           | 18                      |
| 0 0 4  | 5.386          | 5.406           | 16                      |
| 1 0 1  | 3.896          | 3.903           | 23                      |
| 0 0 6  | 3.600          | 3.604           | 8                       |
| 1 0 3  | 3.472          | 3.476           | 6                       |
| 1 0 5  | 2.922          | 2.924           | 100                     |
| perovskite impurity  | 2.870          |                 | 29                      |
| 1 1 0  | 2.803          | 2.806           | 42                      |
| 1 1 2  | 2.713          | 2.716           | 2                       |
| 1 1 4  | 2.490          | 2.490           | 2                       |
| 1 0 7  | 2.437          | 2.437           | 9                       |
| 1 1 6  | 2.163          | 2.162           | 26                      |
| 1 0 9  | 2.056          | 2.055           | 6                       |
| 2 0 0  | 1.985          | 1.984           | 38                      |
| 2 0 2  | 1.952          | 1.951           | 4                       |
| 2 0 4  | 1.864          | 1.862           | 6                       |
| <b><math>H_2SrTa_{1.6}Nb_{0.4}O_7</math> Lamellar Phase</b>                |                |                 |                         |
| <i>(a</i> = 3.89(4), <i>c</i> = 9.87(18) Å)                                |                |                 |                         |
| 001  | 9.88           | 9.88            | 67                      |
| 002  | 4.93           | 9.86            | 20                      |
| 100  | 3.88           | 3.88            | 55                      |
| 110  | 2.75           | 3.89            | 57                      |
| 200  | 1.95           | 3.91            | 100                     |
| <b><math>SrTa_{1.6}Nb_{0.4}O_6</math> Perovskite Phase</b>                 |                |                 |                         |
| <i>(a</i> = 3.93(4) Å)   |                |                 |                         |
| 100  | 3.92           | 3.94            | 41                      |
| 110  | 2.78           | 2.78            | 77                      |
| 200  | 1.97           | 1.97            | 100                     |
| <b><math>SrTa_{1.6}Nb_{0.4}O_6</math> Tetragonal Tungsten Bronze Phase</b> |                |                 |                         |
| <i>(a</i> = 12.47(1), <i>c</i> = 3.897(4) Å)                               |                |                 |                         |
| 210  | 5.575          | 5.577           | 8                       |
| 001  | 3.897          | 3.897           | 49                      |
| 111  | 3.566          | 3.564           | 5                       |
| 320  | 3.457          | 3.459           | 48                      |
| 211  | 3.193          | 3.194           | 44                      |
| 400  | 3.118          | 3.117           | 15                      |
| 410  | 3.024          | 3.024           | 70                      |
| 221  | 2.920          | 2.920           | 25                      |
| 311  | 2.772          | 2.772           | 100                     |
| 321  | 2.587          | 2.587           | 37                      |
| 401  | 2.434          | 2.434           | 6                       |
| 411  | 2.390          | 2.389           | 13                      |
| 331  | 2.346          | 2.346           | 2                       |
| 421  | 2.268          | 2.267           | 4                       |
| 530  | 2.140          | 2.138           | 8                       |
| 620  | 1.972          | 1.971           | 30                      |
| 002  | 1.949          | 1.948           | 23                      |
| 202  | 1.860          | 1.860           | 20                      |
| 601  | 1.834          | 1.834           | 12                      |

400 °C. The disappearance of the layer lines indicates that the condensation of terminal OH groups to form

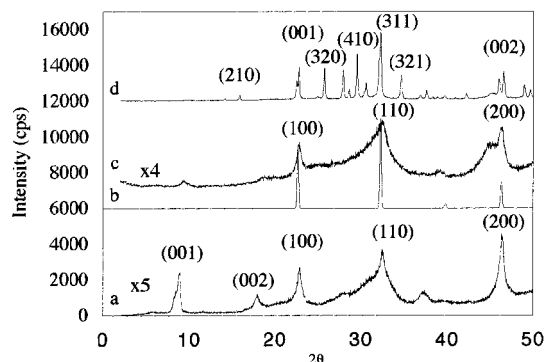


**Figure 3.** (a) Observed X-ray powder diffraction pattern for  $H_2SrTa_{1.6}Nb_{0.4}O_7$ , obtained by proton exchange of  $K_2SrTa_{1.6}Nb_{0.4}O_7$ ; (b) simulated and (c) observed patterns for  $SrTa_{1.6}Nb_{0.4}O_6$  with Sr ions disordered over half the perovskite A sites; (d) observed pattern for the TTB phase obtained by heating perovskite  $SrTa_{1.6}Nb_{0.4}O_6$  to 900 °C.

Ta–O–Ta and Ta–O–Nb linkages between layers also involves motion of  $Sr^{2+}$  into the perovskite A-sites formed in the reaction. The observed powder pattern was accurately simulated as a three-dimensional cubic perovskite, in which  $Sr^{2+}$  occupies half of the available A sites. An ordered structure, in which A sites are occupied and unoccupied in alternate layers, would lead to a progression of layer lines with  $c \approx 2a = 7.86$  Å, and this was not observed. The broadening of the perovskite peaks that accompanies the topochemical dehydration reaction indicates that there are relatively small domains of order in the product. Interestingly, perovskite is the stable polymorph of  $CaTa_2O_6$ , which is made by high-temperature synthesis.<sup>12</sup> Perovskite  $SrTa_2O_6$  and  $SrTa_{2-x}Nb_xO_6$  have not previously been prepared, although unrelated low-temperature orthorhombic phases have been reported.<sup>13</sup> High-temperature synthesis of these compounds invariably yields the tetragonal tungsten bronze (TTB) phase.

Sharp powder diffraction lines from tetragonal  $SrTa_{2-x}Nb_xO_6$  began to grow in at 850–900 °C. The TTB phase was completely formed at 950 °C, as shown in Figure 3. This compound has been previously characterized as isostructural with  $K_{0.57}WO_3$ ,<sup>14,15</sup> and all diffraction lines could be indexed to this phase (Table 1).

Thermal gravimetric analysis/differential thermal analysis (TGA/DTA)<sup>16</sup> and infrared spectroscopy were also used to characterize the phase transitions of  $H_2SrTa_{2-x}Nb_xO_7$  ( $x = 0.0, 0.2, \text{ and } 0.4$ ). IR spectra showed loss of the OH stretching and bending bands (at 3400 and 1700  $cm^{-1}$ , respectively) when the sample was heated to 350 °C for 30 min. The weight loss corresponding to the first phase transition was 1.5, 2.0, and 3.2% (theoretical, 2.8, 2.9, 3.0%) for  $x = 0.0, 0.2, \text{ and } 0.4$ , respectively. Incomplete exchange or partial formation of an amorphous phase is the likely cause of the substoichiometric amount of water lost from the  $x$

(12) (a) Jahnberg, L.; Andersson, S.; Magneli, A. *Acta Chem. Scand.* **1959**, *13*, 1248. (b) Jahnberg, L. *Acta Chem. Scand.* **1963**, *71*, 2548.

(13) (a) Sirotinkin, V. P.; Sirotinkin, S. P. *Russ. J. Inorg. Chem.* **1993**, *38*, 992. (b) Bayer, E.; Gruehn, R. *Z. Anorg. Allg. Chem.* **1984**, *511*, 176.

(14) Francombe, M. H. *Acta Crystallogr.* **1960**, *13*, 131.

(15) Galasso, F.; Katz, L.; Ward, R. *J. Am. Chem. Soc.* **1959**, *81*, 5898.

(16) TGA/DTA was carried out at a heating rate of 10 °C/min in air.

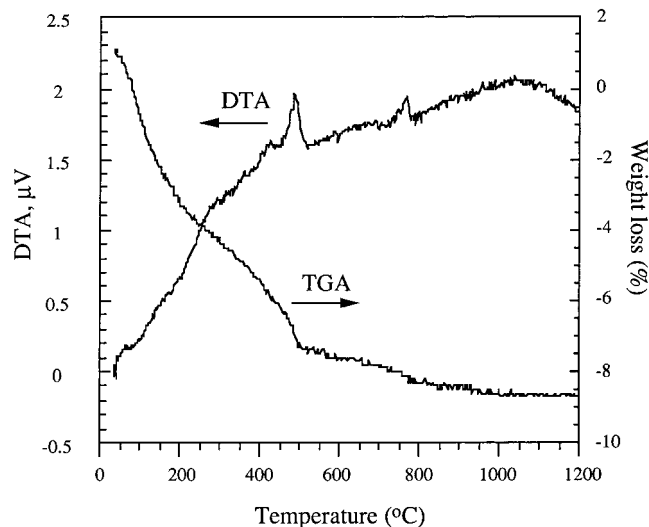


**Figure 4.** DTA and TGA curves for  $\text{H}_2\text{SrTa}_{1.6}\text{Nb}_{0.4}\text{O}_7$  showing dehydration to form perovskite  $\text{SrTa}_{1.6}\text{Nb}_{0.4}\text{O}_6$  and subsequent transformation to the TTB phase.

= 0.0 and 0.2 samples. DTA and TGA data (Figure 4) show that most of the weight loss is gradual but that there is an endothermic DTA peak coincident with the most rapid weight loss at 350–475 °C, and this is coincident with the disappearance of layer lines in the X-ray diffraction pattern. The second phase transition appears as an endotherm at 725 °C, and involves no change in mass because it is a transition between perovskite and tungsten bronze phases of the same composition.

$\text{SrTa}_{2-x}\text{Nb}_x\text{O}_6$  is a member of a large family of metatantalate and metaniobate solid solutions. While both  $\text{SrTa}_2\text{O}_6$  and  $\text{SrNb}_2\text{O}_6$  are nonpolar compounds with the TTB structure, related compounds containing Pb, Sr,

Ba, Ca, and Mg ions are ferroic. Solid solutions of barium and strontium metaniobates (SBN) also adopt the TTB structure, which neither end member exhibits,<sup>12</sup> and have applications in electrooptic,<sup>17</sup> pyroelectric,<sup>18</sup> piezoelectric,<sup>19</sup> and photorefractive<sup>20</sup> devices. Similar applications have been described for  $\text{PbNb}_2\text{O}_6$  solid solutions. The chimie douce reaction described here may provide a route to interesting metastable perovskite solid solutions with the same  $\text{MM}'_2\text{O}_6$  stoichiometries. We also note that similar topochemical reactions should occur for the structurally related Dion–Jacobson phases,<sup>21</sup> which have half the interlayer ion exchange capacity of the Ruddlesden–Popper phases, and for recently described compounds with intermediate ion-exchange capacity.<sup>8b</sup> The ion-exchange/topochemical dehydration reactions of these compounds are currently being investigated and will be reported in a future publication.

**Acknowledgment.** We thank Prof. Darrell Schlom for stimulating discussions. We also thank Mark Palmisano for running the TGA/DTA experiments and Chad Waraksa for help with statistical analysis. This work was supported by grants from the National Science Foundation (CHE-9529202) and DARPA.

CM9802144

(17) Lenzo, P. V.; Spencer, E. G.; Ballman, A. A. *Appl. Phys. Lett.* **1967**, *11*, 23. (b) Ducharme, S.; Feinberg, J.; Neurgaonkar, R. R. *IEEE, J. Quantum Electron.* **1987**, *23*, 2116.

(18) Maciolek, R. B.; Liu, S. T. *J. Electron. Mater.* **1973**, *2*, 191.

(19) Neurgaonkar, R. R.; Kalisher, M. H.; Lim, T. C.; Staples, E. J.; Keester, K. I. *Mater. Res. Bull.* **1980**, *15*, 1235.

(20) Neurgaonkar, R. R.; Cross, L. E. *Mater. Res. Bull.* **1986**, *21*, 893.

(21) (a) Dion, M.; Ganne, M.; Tournoux, M. *Mater. Res. Bull.* **1981**, *16*, 1429. (b) Jacobson, A. J.; Johnson, J. W.; Lewandowski, J. T. *Inorg. Chem.* **1985**, *24*, 3727–3729. (c) Treacy, M. M. J.; Rice, S. B.; Jacobson, A. J.; Lewandowski, J. T. *Chem. Mater.* **1990**, *2*, 279.